Aeroelastic response of helicopter rotors using a 3D unsteady aerodynamic solver

M. Gennaretti and G. Bernardini
University Roma Tre
Department of Mechanical and Industrial Engineering
Rome, Italy

ABSTRACT

The prediction of blade deflections and vibratory hub loads concerning helicopter main rotors in forward flight is the objective of this work. They are determined by using an aeroelastic model derived through the coupling between a nonlinear blade structural model and a boundary integral equation solver for three-dimensional, unsteady, potential aerodynamics. The Galerkin method is used for the spatial integration, whereas the periodic blade response is determined by a harmonic balance approach. This aeroelastic model yields a unified approach for aeroelastic response and blade pressure prediction that may be used for aeroacoustic purposes, with the possibility of including effects from both blade-vortex interaction and multiple-body aerodynamic interaction. Quasi-steady aerodynamic models with wake-inflow from the three-dimensional aerodynamic solver are also applied, in order to perform a comparative study. Numerical results show the capability of the aeroelastic tool to evaluate blade response and vibratory hub loads for a helicopter main rotor in level flight conditions, and examine the sensitivity of the predictions on the aerodynamics model used.

NOMENCLATURE

a	lift curve slope
b	section semi-chord length
c_D	section drag coefficient
C	profile contour
C_n	section normal force coefficient
e_h	dimensionless hinge offset
f_n^v, f_n^w, f_n^ϕ	shape functions
$f_{aer_j}^v, f_{aer_j}^w, f_{aer_j}^\phi$	generalised aerodynamic forces
$\mathbf{f}_{aer}$	vector of the generalised aerodynamic forces
G	Green's function
L_v, L_w	dimensionless generalised aerodynamic forces per unit length
M_ϕ	dimensionless aerodynamic pitching moment per unit length
M, C, K	mass, damping and stiffness matrices
n	unit normal on a surface
p	dimensionless pressure
q_n^v, q_n^w, q_n^ϕ	generalised co-ordinates
q	vector of the generalised co-ordinates
S_B,S_W	body and wake surfaces
u_T,u_P	blade section velocity components
v,w	displacements of the elastic axis
v	fluid velocity
x	dimensionless blade span co-ordinate
x_R	dimensionless aerodynamic root cutout
$\boldsymbol{x}$,$\boldsymbol{y}$	observer and source locations

Paper No. 3022. Manuscript received 26 September 2005, revised 17 July 2006 accepted 25 August 2006.

https://doi.org/10.1017/S0001924000001664 Published online by Cambridge University Press

y,z	dimensionless lag-wise and flap-wise section co-ordinate
β_{pc}	blade precone angle
γ	Lock number
θ	pitch angle
κ	dimensionless torsion rigidity
Λ_1, Λ_2	dimensionless flap and lead-lag bending stiffnesses
$\bar{\mu}_1, \bar{\mu}_2, \bar{\mu}$	dimensionless mass radii of gyration
ϕ	elastic torsion deflection
φ	velocity potential
Ω	blade angular velocity
ω	blade section angular velocity in the rotating frame

Symbols

$()\hat{}$	Fourier domain
$\dot{()}$	time derivative
$()'$	space derivative

1.0 INTRODUCTION

This paper deals with an aeroelastic prediction tool obtained by coupling a nonlinear blade structural dynamics model with a three-dimensional unsteady aerodynamic solver. It is aimed to the prediction of the blade response and vibratory hub loads concerning helicopter main rotors in forward flight. Indeed, rotational and translational motion combined with the resulting complex aerodynamic environment in which helicopter rotors operate cause blade periodic elastic deformations and transmission of vibratory loads at the hub and hence at the fuselage.

The availability of a reliable tool for the prediction of blade deformations and vibrating hub loads is of primary interest in the helicopter design. Blade deflections play an important role in the occurrence of blade-vortex interaction (BVI), which is the source both of severe acoustic annoyance produced by helicopters during maneuvers like, for instance, descent flight, and of higher harmonic airloading that are transmitted at the hub. Hub loads are sources of fuselage vibrations. They produce acoustic disturbances inside the cabin that may cause unacceptable ride discomfort, and have also a significant impact on the fatigue-life of the structure (and hence on maintenance costs). The prediction of the aeroelastic response of helicopter rotor blades requires the introduction of accurate structural and aerodynamic models. In particular, the structural model has to take into account both the strong coupling between bending and torsion degrees of freedom of the blade and the nonlinearities arising from the significant deformations usually experienced by slender rotor blades. The aerodynamic modeling has to be able to describe three-dimensional, unsteady effects, with particular attention on the prediction of wake contribution, which is of crucial importance in the aerodynamics of helicopter rotors.

In the last decades, the work of many researchers has been addressed to the prediction of aeroelastic response with the aim of examining both BVI noise and vibrating hub loads. Typically, prediction tools developed to analyze rotor aeroelasticity are based on aerodynamic models that couple 2D airfoil-theory loads with wake inflow from a 3D free-wake solver. If blade pressures are needed for aeroacoustic computations, these are usually determined from a different aerodynamic tool having blade deformations among the required inputs. An example of this kind of approach is the study aimed to aeroelastic applications presented in Ref. 1, where a multiple-trailer vortex model is used in the free-wake analysis that predicts the wake inflow to be coupled with an aerodynamic load model based on thin airfoil theories. A similar approach is considered in Ref. 2 for aeroacoustic purposes. The combined use of a dual vortex free-wake code with a 2D aerodynamics code is applied in Refs 3 and 4 for the aeroelastic and aeroacoustic analysis of rotors aimed to vibration and noise reduction. In Ref. 5 the aerodynamic analysis of rotors in BVI conditions consists of a four-step procedure. An initial rotor trim code based on 2D aerodynamics is followed by a vortex-lattice free-wake analysis, that is then coupled with a roll-up model in order to identify the higher-intensity vortex structures. In turn, these are considered as the interacting vortices in a pressure predictor code based on a 2D solver. Predictions of vibratory hub load through an aeroelastic tool combining unsteady 2D section load models with wake inflow from free-wake analysis are presented in Ref. 6. An extensive review on tools available for vibratory hub load prediction is given in Ref. 7.

Here, the attention is focused on the development of an aeroelastic model that uses 3D, unsteady aerodynamics. It is obtained by coupling the equations of blade dynamics introduced by Hodges and Dowell in Ref. 8, with the aerodynamic solution given by a 3D Boundary Element Method (BEM) for potential flows (see Refs 9 and 10). The resulting integro-differential equations are solved through a Galerkin approach in space, followed by a harmonic balance method for the identification of the periodic blade deformation arising in forward flight conditions. The 3D aerodynamic solver may be applied either for the direct evaluation of the generalised aerodynamic loads, or for the calculation of the wake inflow to be combined with a 2D section load modeling. In both cases, for noise evaluation goals, it can be used also to obtain the blade pressure to be used in an aeroacoustic solver. Thus, such prediction tool yields a unified approach for aeroelastic response and blade pressure prediction to be used for aeroacoustic purposes, with the possibility of including effects from both BVI and multiple-body aerodynamic interaction (see Refs 11 and 12). The structural dynamics and aerodynamics formulations are outlined in Sections 2.0 and 3.0, respectively, whereas Section 4.0 describes the technique applied to integrate the resulting aeroelastic model. Numerical results concerning a helicopter main rotor in level flight conditions are discussed in Section 5.0. They are aimed both to the validation of the aeroelastic tool and to the assessment of the effects of the aerodynamic models on aeroelastic predictions.

2.0 BLADE STRUCTURAL DYNAMICS MODEL

The blade structural dynamics is described through the nonlinear flap-lag-torsion equations of motion presented in Ref. 8 by Hodges and Dowell. These are based on a beam-like model and are valid for straight, slender, homogeneous, isotropic, nonuniform, twisted blades, undergoing moderate displacements. Indeed, second order terms are retained in the equations after the application of an ordering scheme that drops third-order terms (with respect to bending slope) not contributing to damping. Then, eliminating the radial displacement from the set of equations by solving it in terms of local tension, for mass and tensile axes coinciding with the elastic axis and a uniform mass distribution, the lead-lag, $v(x,t)$, and flap, $w(x,t)$, displacements of the elastic axis, along with the blade cross-section elastic rotation (torsion), $\phi(x,t)$, about the deformed elastic axis are governed by the following set of three dimensionless integro-differential equations

$$\left[\left(\Lambda_2-\Lambda_{21}\mathrm{Sin}^2\theta\right)v''\right]''+\frac{\Lambda_{21}}{2}\left[w''\,\mathrm{Sin}\left(2\theta\right)\right]''+\Lambda_{21}\left[\phi\,w''\mathrm{Cos}\left(2\theta\right)-\phi\,v''\mathrm{Sin}\left(2\theta\right)\right]''-\left[v'\int_x^1\left(\bar{x}+2\dot{v}\right)\mathrm{d}\bar{x}\right]'$$
$$-2\int_{e_h}^{x}\left(v'\dot{v}'+w'\dot{w}'\right)\mathrm{d}\bar{x}+\ddot{v}-v-2\beta_{pc}\dot{w}-e_h\left[v'\left(1-x\right)\right]'=L_v \qquad \ldots(1)$$

$$\left[\left(\Lambda_1-\Lambda_{21}\mathrm{Sin}^2\theta\right)w''\right]''+\frac{\Lambda_{21}}{2}\left[v''\,\mathrm{Sin}\left(2\theta\right)\right]''+\Lambda_{21}\left[\phi\,v''\mathrm{Cos}\left(2\theta\right)+\phi\,w''\mathrm{Sin}\left(2\theta\right)\right]''-\left[w'\int_x^1\left(\bar{x}+2\dot{v}\right)\mathrm{d}\bar{x}\right]'$$
$$+\ddot{w}+2\beta_{pc}\dot{v}+\beta_{pc}x-e_h\left\{\left[w'\left(1-x\right)\right]'-\beta_{pc}\right\}=L_w \qquad \ldots(2)$$

$$-\frac{\bar{\mu}^2K}{2}\left[\phi'\left(1-x^2\right)\right]'-\left(\kappa\phi'\right)'+\bar{\mu}^2\ddot{\phi}+\phi\left(\bar{\mu}_2^2-\bar{\mu}_1^2\right)\mathrm{Cos}\left(2\theta\right)-e_h\bar{\mu}^2K\left[\left(\theta+\phi\right)'\left(1-x\right)\right]'$$
$$-\bar{\mu}^2K\left[\theta'\int_x^1\left(\bar{x}+2\dot{v}\right)\mathrm{d}\bar{x}\right]'+\Lambda_{21}\left[\left(w''^2-v''^2\right)\mathrm{Sin}\theta\,\mathrm{Cos}\theta+v''w''\mathrm{Cos}\left(2\theta\right)\right]+\left(\bar{\mu}_2^2-\bar{\mu}_1^2\right)\frac{\mathrm{Sin}\left(2\theta\right)}{2}=M_\phi \qquad \ldots(3)$$

where x denotes the spanwise location and θ is the pitch angle

https://doi.org/10.1017/S0001924000001664 Published online by Cambridge University Press

distribution (see Fig. 1). In the equations above, dimensionless lengths are related to the blade radius, R, and dimensionless time coincides with blade azimuth position. Thus, the dimensionless bending equations have been obtained by division by the parameter $m\Omega^2R^2$ while the dimensionless torsion equation is the result of the division by the parameter $m\Omega^2R^3$, with m denoting the blade mass per unit length and Ω denoting the angular velocity of the blade. In addition, Λ_1 and Λ_2 are the dimensionless flap and lead-lag bending stiffnesses, respectively, $\Lambda_{12} = \Lambda_2 - \Lambda_1$, κ is the dimensionless torsion rigidity, $\bar{\mu}_1$, $\bar{\mu}_2$, $\bar{\mu}$ are the dimensionless sectional mass radii of gyration ($\bar{\mu} = \sqrt{\bar{\mu}_1^{\,2} + \bar{\mu}_2^{\,2}}$), K is the square of the ratio between the blade cross-section polar radius of gyration and the blade cross-section mass radius of gyration, whereas β_{pc} is the blade precone angle and e_h denotes the hinge offset. The forcing terms in the first two equations, L_v and L_w, are the dimensionless generalised aerodynamic forces per unit length, whereas M_ϕ is the dimensionless aerodynamic pitching moment per unit length (for details on the definition of the quantities appearing in Equations (1-3), see Ref. 13).

3.0 ROTOR POTENTIAL AERODYNAMICS

The three-dimensional unsteady aerodynamic model used in this work is obtained through a boundary integral approach for potential, incompressible flows. It is based on the formulation introduced in Ref. 9, and on the free-wake algorithms presented in Ref. 14 for hovering rotors and in Ref. 10 for rotors in forward flight.

For φ denoting the velocity potential function (i.e. such that the velocity field is given by $\mathbf{v} = \nabla\varphi$), the potential-field solution for the arbitrary motion of a lifting body may be obtained through the following boundary integral representation

$$\varphi(\mathbf{x},t) = \int_{S_B}\left(\frac{\partial\varphi}{\partial n}G - \varphi\frac{\partial G}{\partial n}\right)\mathrm{d}S(\mathbf{y}) - \int_{S_W}\Delta\varphi\left(\mathbf{x}_{TE}, t-\tau\right)\frac{\partial G}{\partial n}\mathrm{d}S(\mathbf{y}) \quad \ldots (4)$$

where S_B denotes the body surface, and S_W denotes the zero-thickness wake surface where the vorticity generated by the body remains confined. In addition, $G = -1/4\,\pi\|\mathbf{x} - \mathbf{y}\|$ is the fundamental solution of the Laplace equation, $\partial/\partial n = \mathbf{n}\cdot\nabla$ with $\mathbf{n}$ denoting the outward unit normal to the body surface, whereas $\Delta\varphi$ ($\mathbf{x}_{TE}$, $t - \tau$) is the potential discontinuity at the trailing edge location where the wake point was released at the delayed time $t - \tau$. Furthermore, the application of the body surface impermeability condition yields the Neumann boundary condition, $\partial\varphi/\partial n = \mathbf{v}_B\cdot\mathbf{n}$, where $\mathbf{v}_B$ denotes the velocity of the body surface points, given by the sum of the rigid-body motion with that due to the body elastic deformation. For $\mathbf{x}$ approaching S_B, Equation (4) yields an integral equation which may be used to obtain the values of φ on S_B, since $\partial\varphi/\partial n$ is known from the boundary condition (see, for instance, Refs 9 and 10). Equation (4) is solved numerically by boundary elements, i.e. by discretising S_B and S_W into quadrilateral panels, assuming φ, $\partial\varphi/\partial n$ and $\Delta\varphi$ to be piecewise constant (zero-th order, boundary element method – BEM), and imposing that the equation be satisfied at the center of each body element (collocation method).

Once the potential on the body surface has been determined, the Bernoulli theorem yields the pressure distribution, p, and hence the aerodynamic forces acting on it may be evaluated. For the problem under examination, the distributed loads in Equations (1), (2) and (3) are obtained from the following expressions (where dimensionless quantities are used)

$$L_v = -\int_C p\,n_v\,\mathrm{d}\ell, \quad L_w = -\int_C p\,n_w\,\mathrm{d}\ell, \quad M_\phi = -\int_C p\,(y n_w + z n_v)\,\mathrm{d}\ell, \quad \ldots (5)$$

where C denotes the section profile contour, and n_v and n_w denote the $\mathbf{n}$– components that are parallel to lead-lag and flap displacements, respectively (the y co-ordinate is aligned with the lead-lag displacement, whereas the z co-ordinate is aligned with the flap displacement, both having the origin at the elastic axis).

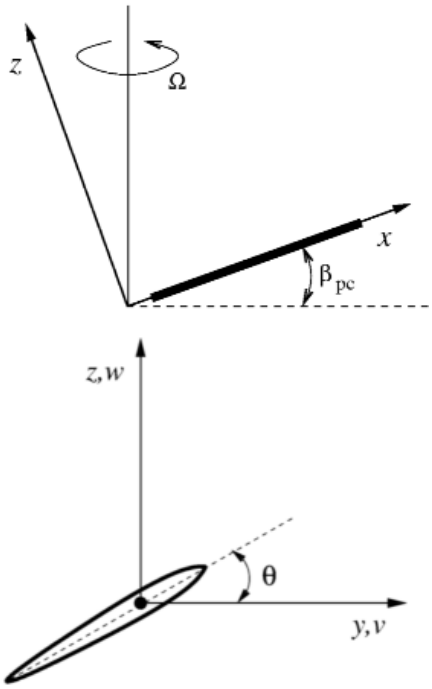


Figure 1. Co-ordinate system and deflections of the rotor blade.

This aerodynamic formulation may be applied both with prescribed wake shapes and for free-wake analysis. In the free-wake approach, the shape of the wake, S_W, is obtained as part of the solution. Indeed, once φ on the surface is known, the application of the gradient operator to Equation (4) yields an integral representation of the velocity field. Thus, at each step of the time-marching procedure, the wake points are moved accordingly to the local velocity field and the shape of S_W is continuously renewed.

Note that, if the helicopter rotor is in strong BVI (Blade-Vortex Interaction) conditions the formulation presented above cannot be applied as it is. This occurs because of instabilities of the numerical scheme produced both by inaccuracies in the evaluation of the contribution of the wake panels impinging the body and by the unrealistic modeling of BVI when a zero-thickness wake is used (the local vorticity distribution is strongly influenced by viscosity). In this case, the boundary-integral formulation presented in Ref. 11 as an extension of the one outlined above should be applied.

3.1 Other aerodynamic formulations

In several rotor prediction tools that are commonly used by helicopter industries, the aeroelastic response of a helicopter rotor is analyzed by using two-dimensional, quasi-steady aerodynamic models with inclusion of wake-inflow (mainly, to take into account 3D trailing vortices effect). These are based on the section loads given either by the Greenberg theory (see Ref. 15) or by the Theodorsen theory (see Ref. 16) under the assumption of very low frequency analysis, for which the lift deficiency function is constant and equal to one. This restriction implies that the influence of unsteady shed vortices on the 2D theoretical solutions is neglected and introduces some simplification in the numerical analysis, in that avoids the computation of convolution integrals.

Denoting with u_T and u_P the 3/4-chord point dimensionless velocity components in the plane that is parallel to the section principal axes (u_T is chordwise), and with $\alpha = \theta + \phi$ the section rotation, the distributed aerodynamic loads in Equations (1-3) as derived from the quasi-steady Greenberg theory are given by (see also Ref. 13)

$$L_v = \frac{\gamma}{6}\left[u_P\left(u_P + b\,\omega + u_T\,\alpha\right) - \frac{c_D}{a}u_T^2 + \frac{b}{2}\dot{u}_P\,\alpha - \left(\frac{b}{2}\right)^2\dot{\omega}\,\alpha\right] \quad \ldots (6)$$

https://doi.org/10.1017/S0001924000001664 Published online by Cambridge University Press

$$L_w = -\frac{\gamma}{6}\left[u_P\left(u_T - b\omega\alpha - u_p\,\alpha\right) + \frac{c_D}{a}u_T^2\,\alpha + \frac{b}{2}\dot{u}_P + \left(\frac{b}{2}\right)^2\dot{\omega}\right] \quad \ldots (7)$$

$$M_\phi = -\frac{\gamma}{6}\left(\frac{b}{2}\right)^2\left(u_T\omega - \dot{u}_P - \frac{b}{4}\dot{\omega}\right) \quad \ldots (8)$$

where $\gamma = 6\,\rho\,a\,b\,R/m$ is the Lock number (with ρ denoting air density), b is the dimensionless section semi-chord length, a is the lift curve slope, C_D is the section drag coefficient, and ω is the dimensionless section angular velocity about the deformed elastic axis. The velocity components, u_T and u_P, are the result of the combination of rigid blade motion and elastic deformation (therefore, they depend also on v,w,ϕ), and the effects of the inflow velocity induced by the wake vorticity are included in the u_P component. Note that Equation (8) expresses the pitching moment about the 1/4-chord point.

Here, two quasi-steady aerodynamic models are examined in the numerical investigation. One is obtained by using the wake inflow described by the Drees linear analytical model presented in Ref. 17, whereas the second is obtained by applying the wake-inflow predicted by the BEM solution discussed above.

4.0 HARMONIC BALANCE FOR AEROELASTIC RESPONSE

Equations (1), (2) and (3) governing the blade structural dynamics coupled with the aerodynamic models describing the unsteady forcing terms yield the aeroelastic integro-differential model to be integrated.

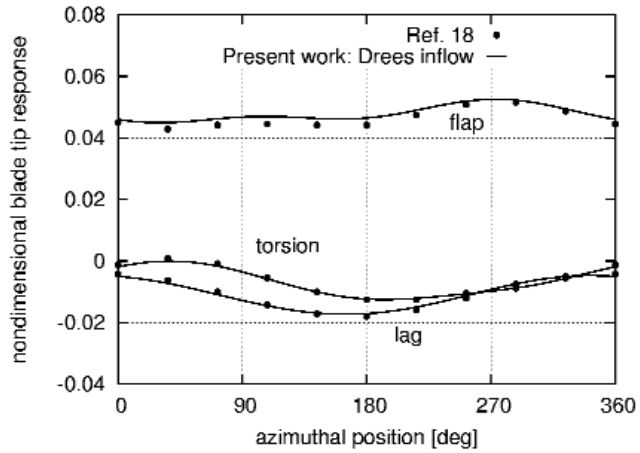


Figure 2. Blade deformation (μ = 0·15).

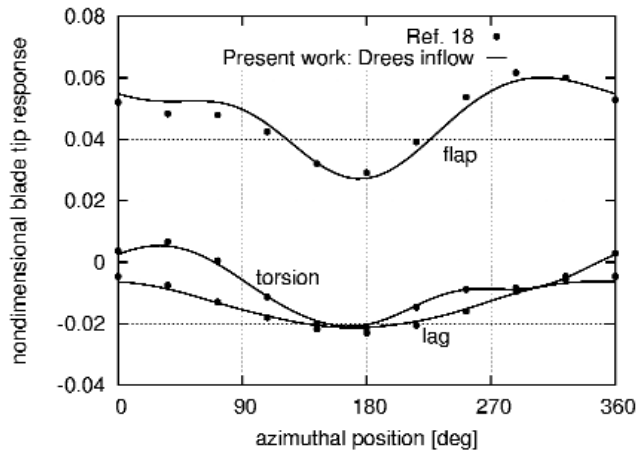


Figure 3. Blade deformation (μ = 0·30).

Here, the space discretisation is performed through the Galerkin method, starting from the following description of the elastic deformation as a linear combination of shape functions

$$v(x,t) = \sum_n q_n^v(t) f_n^v(x), \quad w(x,t) = \sum_n q_n^w(t) f_n^w(x)$$

$$\phi(x,t) = \sum_n q_n^\phi(t) f_n^\phi(x), \quad \ldots (9)$$

Following Ref. 13, f_n^v and f_n^w have been chosen as the bending natural modes of vibration of the non-rotating beam, Ψ_n, whereas f_n^ϕ have been chosen as the torsion natural modes of vibration of the non-rotating beam, Θ_n. The resulting aeroelastic system consists of a set of nonlinear ordinary differential equations of the type

$$\mathbf{M}(t)\,\ddot{\mathbf{q}} + \mathbf{C}(t)\,\dot{\mathbf{q}} + \mathbf{K}(t)\,\mathbf{q} = \mathbf{f}_{str}^{nl}(t,\mathbf{q}) + \mathbf{f}_{aer}(t,\mathbf{q}) \quad \ldots (10)$$

where $\mathbf{q}$ denotes the vector of the Lagrangean co-ordinates (modal amplitudes), whereas $\mathbf{M}$, $\mathbf{C}$ and $\mathbf{K}$ are time-periodic, mass, damping, and stiffness structural matrices representing the linear structural terms (note that these matrices are time-variant because of the cyclic pitch). Nonlinear structural contributions are collected in the forcing vector $\mathbf{f}_{str}^{nl}(t,\mathbf{q})$ whereas vector $\mathbf{f}_{aer}(t,\mathbf{q})$ collects the generalised aerodynamic forces. Specifically, the generalised forces related to lead-lag, flap, and torsion equations are, respectively, given by

$$f_{aer_j}^v = \int_{x_R}^1 L_v\,\Psi_j\,\mathrm{d}x, \quad f_{aer_j}^w = \int_{x_R}^1 L_w\,\Psi_j\,\mathrm{d}x, \quad f_{aer_j}^\phi = \int_{x_R}^1 M_\phi\,\Theta_j\,\mathrm{d}x \quad \ldots (11)$$

where x_R is the dimensionless aerodynamic root cutout.

Since the aim of this work is the aeroelastic response of helicopter rotors in forward flight conditions, the system in Equation (10) is solved by using the harmonic balance approach. It is a methodology suitable for the analysis of the asymptotic solution (as time goes to infinity) of differential equations forced by periodic terms, as in the present case. The harmonic balance solution consists of: (*i*) express LHS and RHS of the aeroelastic system (Equation (10)) in terms of their Fourier series; (*ii*) equate the resulting coefficients; (*iii*) solve the corresponding algebraic system in terms of the unknown Fourier coefficients of the Lagrangean co-ordinates of the problem. Specifically, expressing $\mathbf{q}$ and $\mathbf{f} = \mathbf{f}_{str}^{nl} + \mathbf{f}_{aer}$ in terms of the following Fourier series

$$\mathbf{q}(t) = \mathbf{q}_0 + \sum_{n=1}^{N}\left[\mathbf{q}_n^c \mathrm{Cos}(\Omega_n t) + \mathbf{q}_n^s \mathrm{Sin}(\Omega_n t)\right] \quad \ldots (12)$$

$$\mathbf{f}(t) = \mathbf{f}_0 + \sum_{n=1}^{N}\left[\mathbf{f}_n^c \mathrm{Cos}(\Omega_n t) + \mathbf{f}_n^s \mathrm{Sin}(\Omega_n t)\right] \quad \ldots (13)$$

(where $\mathbf{q}_n^c$, $\mathbf{q}_n^s$, $\mathbf{f}_n^c$ and $\mathbf{f}_n^s$ denote cosine and sine components of the n-th harmonic of $\mathbf{q}$ and $\mathbf{f}$, whereas $\Omega_n = n\Omega$, with Ω representing the fundamental frequency, i.e. the rotor angular velocity) and then combining with Equation (10) yields the following periodic aeroelastic solution in terms of the sine and cosine harmonic components

$$\hat{\mathbf{q}} = \left[\hat{\mathbf{M}} + \hat{\mathbf{C}} + \hat{\mathbf{K}}\right]^{-1}\hat{\mathbf{f}} \quad \ldots (14)$$

where $\hat{\mathbf{q}}^T = \left\{\mathbf{q}_0\,\mathbf{q}_1^c\,\mathbf{q}_1^s\,\mathbf{q}_2^c\,\mathbf{q}_2^s\cdots\right\}$ and $\hat{\mathbf{f}}^T = \left\{\mathbf{f}_0\,\mathbf{f}_1^c\,\mathbf{f}_1^s\,\mathbf{f}_2^c\,\mathbf{f}_2^s\cdots\right\}$. Matrices $\hat{\mathbf{M}}$, $\hat{\mathbf{C}}$ and $\hat{\mathbf{K}}$ in Equation (14) come out from Equation (10) by combining the harmonics of the $\ddot{\mathbf{q}}$, $\dot{\mathbf{q}}$ and $\mathbf{q}$ terms with the harmonics of the matrices $\mathbf{M}$, $\mathbf{C}$ and $\mathbf{K}$. In particular, if $\mathbf{M}$, $\mathbf{C}$ and $\mathbf{K}$ were constant matrices, in Equation (14) one would have block-diagonal matrices and each harmonic of $\mathbf{q}$ would depend only on the same harmonic of $\mathbf{f}$ (the $\mathbf{q}$-harmonics equations would be uncoupled). On the contrary, in the problem under examination the structural matrices are periodic and hence, once expressed in terms of the Fourier series and combined with

https://doi.org/10.1017/S0001924000001664 Published online by Cambridge University Press

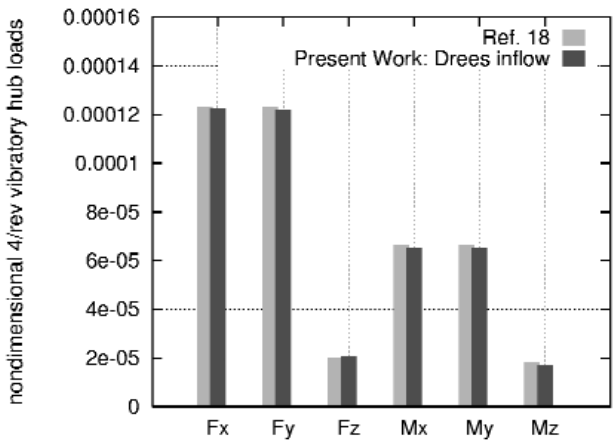


Figure 4. 4/rev hub loads (μ = 0·30).

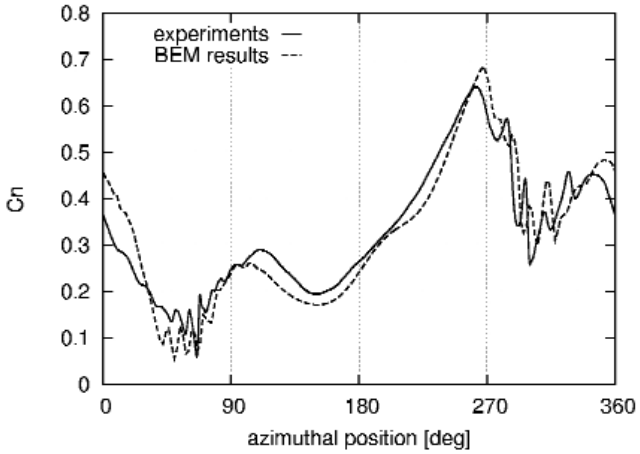


Figure 5. C_n at blade section x = 0·92.

the harmonics of $\ddot{\mathbf{q}}$, $\dot{\mathbf{q}}$ and $\mathbf{q}$ they yield fully-populated $\hat{\mathbf{M}}$, $\hat{\mathbf{C}}$ and $\hat{\mathbf{K}}$ matrices. Thus, the algebraic equations for the unknown harmonics of $\mathbf{q}$ appearing in Equation (14) are coupled with each other (as an example, in Appendix the $\hat{\mathbf{K}}$ matrix is given in terms of the harmonics of $\mathbf{K}$).

Because of the presence of nonlinear terms and because of the application of the BEM aerodynamic solver (i.e. a solver that does not yield an explicit relation between Lagrangean variables and aerodynamic forces), Equation (14) has to be solved using an iterative procedure. Starting from an initial-guess periodic blade deformation, $\hat{\mathbf{q}}$, first the corresponding nonlinear structural terms, $\mathbf{f}_{str}^{nl}$, and aerodynamic boundary conditions are calculated. Then, periodic aerodynamic forces $\mathbf{f}_{aer}$ are evaluated and the harmonics of $\mathbf{f} = \mathbf{f}_{str}^{nl} + \mathbf{f}_{aer}$ (i.e. $\hat{\mathbf{f}}$) are used in Equation (14) to obtain a new blade deformation. In turn, this yields new sets of nonlinear structural terms and aerodynamic forces and the procedure is applied until convergence is reached (i.e. two subsequent iterations give the same blade deformation within the limits of the required accuracy).

Note that, the convergence of the iterative procedure based on Equation (14) is not assured. In order to make the iterative algorithm converge or, anyway, to speed up the convergence process, it is convenient to introduce the aerodynamic Jacobian, $\hat{\mathbf{J}}_{aer}$, such that $\hat{\mathbf{f}}_{aer} = \hat{\mathbf{f}}_{aer}^{0} + \hat{\mathbf{J}}_{aer}\,\hat{\mathbf{q}} + \hat{\mathbf{f}}_{aer}^{nl}$ with $\hat{\mathbf{f}}_{aer}^{0}$ denoting the aerodynamic load portion that is not influenced by the structural deformation. The Jacobian, $\hat{\mathbf{J}}_{aer}$, can be evaluated either analytically or numerically, the choice depending on the aerodynamic solver applied. The corresponding harmonic aeroelastic solution is obtained from convergence of an iterative procedure applied to the following nonlinear equation (that replaces Equation (14))

$$\hat{\mathbf{q}} = \left[\hat{\mathbf{M}} + \hat{\mathbf{C}} + \hat{\mathbf{K}} - \hat{\mathbf{J}}_{aer}\right]^{-1} \hat{\mathbf{f}} \qquad \ldots (15)$$

where $\hat{\mathbf{f}} = \hat{\mathbf{f}}_{str}^{nl} + \hat{\mathbf{f}}_{aer}^{0} + \hat{\mathbf{f}}_{aer}^{nl}$ For the sake of computational efficiency it is possible to consider a constant aerodynamic Jacobian, corresponding to the one at $\hat{\mathbf{q}} = \mathbf{0}$: this limits the application of the aerodynamic solver (that could be time costly) and implies the need of only one matrix inversion (see Equation (15)). In this case, the solution of Equation (15) through iterative procedure would correspond to the application of the Newton-Raphson method with a constant-Jacobian approximation.

5.0 NUMERICAL RESULTS

In this section, some numerical results are presented in order to validate the aeroelastic procedure presented above, as well as to investigate the impact of the aerodynamic modeling on the prediction of the aeroelastic response of helicopter rotors. Specifically, following Ref. 18, a rotor having four rectangular blades with radius R = 4·93m, chord c = 0·395m, and a linear twist angle of –8°, has been examined in level flight, at advance ratios μ = 0·15 and μ = 0·30. The rotational speed of the rotor is Ω = 40rad/s. The sectional rotor structural properties considered in the analysis are (see also Ref. 18) Λ_1 = 0·008345, Λ_2 = 0·023198, κ = 0.00225 $\bar{\mu}_1$ = 0·01, $\bar{\mu}_2$ = 0·02, m = 6·462kg/m. In addition, the hinge offset is e_h = 0·04 and the aerodynamic root cutout is equal to x_R = 0·1 . For the two advance ratios investigated, shaft, collective and cyclic pitch angles of the rotor blades are those determined in Ref. 18 with linear inflow.

First, in order to validate the aeroelastic prediction tool presented here, the numerical results are compared with those presented in Ref. 18, which are based on the rotor code UMARC (see Ref. 19) that is a well-known, widely-used aeroelastic solver. It uses a nonlinear, finite-element approach for the structural analysis, whereas unsteady aerodynamic loads are given by combination of 2D airfoil theory with wake inflow obtained either from analytical models or from free-wake analysis (see, for instance, Refs 6 and 19). In this case, in order to introduce similar approximations in the aerodynamic load description as in Ref. 18, the 2D quasi-steady aerodynamics with linear Drees wake inflow has been applied. Figures 2 and 3 show that, for both advance ratios examined, the blade tip deformations (namely, lag, flap and torsion) predicted by the aeroelastic tool presented here are in good agreement with those presented in Ref. 18. The same level of agreement is shown in Fig. 4 in which, for the advance ratio μ = 0·30, the comparison is presented in terms of the 4/rev vibrating loads calculated at the rotor hub (it is worth noting that the hub is forced by the combination of the loads transmitted by each rotor blade, and the harmonics of the resulting loads are multiples of the number of the rotor blades). These results have been obtained by using five modes and five harmonics for the description of each elastic degree of freedom, and the same number of modes and harmonics has been used also for the aeroelastic predictions presented in the following.

The BEM solver has been validated in the past both for steady and unsteady rotor configurations (see, for instance, Refs 20 and 21). Here, a validation with experimental results obtained within the European Project HELISHAPE (see Ref. 22) is presented in Figs 5 and 6. It concerns the four-bladed EC/ONERA 7A main rotor in a 6° –descent flight configuration, for which the formulation presented in Ref. 11 has been applied. These figures show the comparisons between measurements and free-wake BEM predictions in terms of the normal force

https://doi.org/10.1017/S0001924000001664 Published online by Cambridge University Press

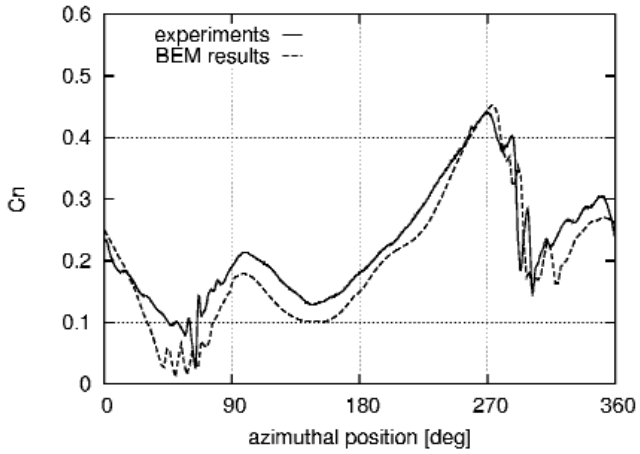


Figure 6. C_n at blade section x = 0·98.

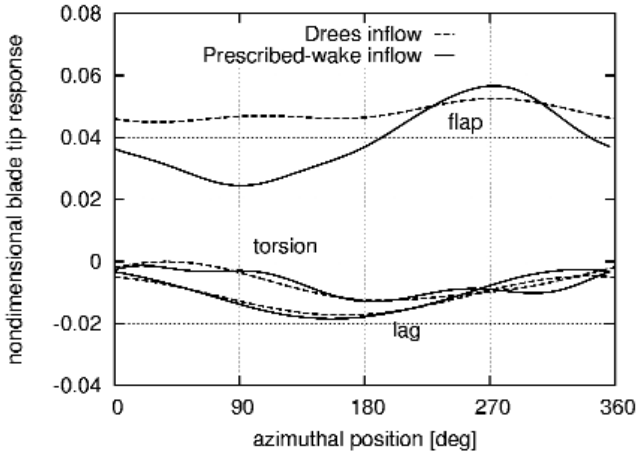


Figure 7. Blade deformation: linear inflow *vs* prescribed-wake inflow (μ = 0·15).

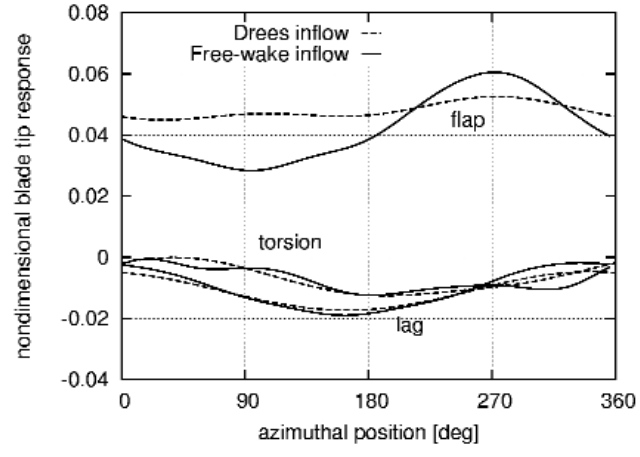


Figure 8. Blade deformation: linear inflow vs free-wake inflow (μ = 0·15).

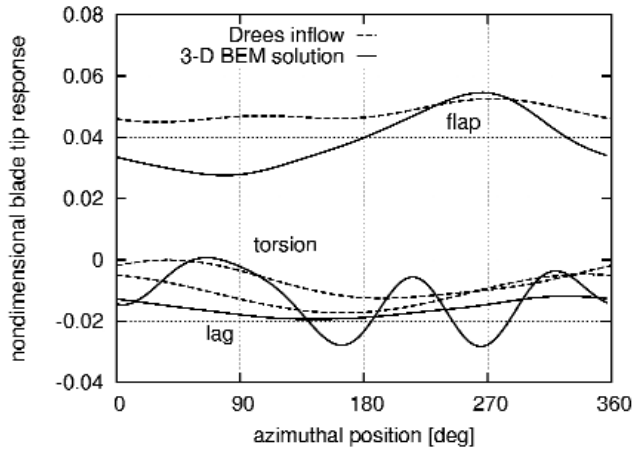


Figure 9. Blade deformation: linear inflow *vs* 3D BEM solution (μ = 0·15).

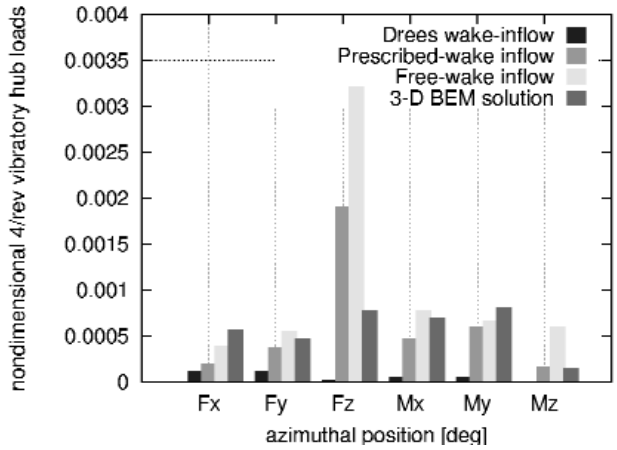


Figure 10. 4/rev hub loads (μ = 0·15).

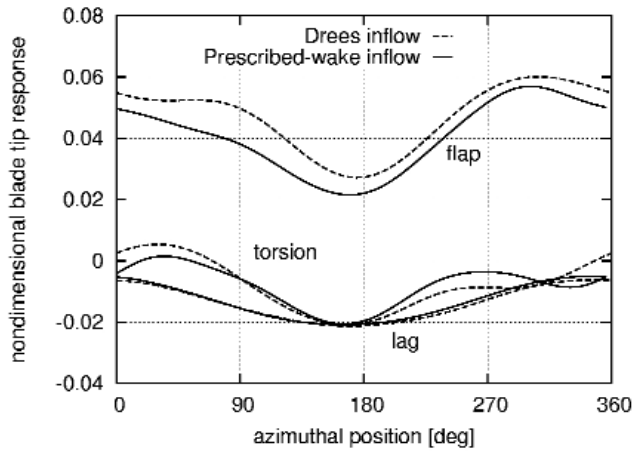


Figure 11. Blade deformation: linear inflow *vs* prescribed-wake inflow (μ = 0·30).

https://doi.org/10.1017/S0001924000001664 Published online by Cambridge University Press

coefficient, C_n, respectively at blade sections $x = 0{\cdot}92$ and $x = 0{\cdot}98$. These results demonstrate that the BEM solver has a good capability of prediction of unsteady airloads, with inclusion of BVI effects that are well captured both in terms of oscillation amplitude and in terms of azimuth location occurrence. In the past the BEM solver has been applied also to determine the wake inflow to be combined with 2D quasi-steady aerodynamics. The resulting aeroelastic model has been validated in Ref. 23 by comparing its predictions with the experimental data provided by the HART II program, which concerns a scaled model of the Bo105 main rotor (see, for instance, Ref. 24).

Now, the attention is focused on the examination of the effects of the aerodynamic model on the aeroelastic response prediction. Specifically, in addition to the use of 2D quasi-steady aerodynamics with linear wake inflow presented in Figs 2-4, elastic blade deformations and vibrating hub loads have been predicted using also: (*i*) 2D quasi-steady aerodynamics with wake inflow from the BEM solver with a prescribed wake shape, (*ii*) 2D quasi-steady aerodynamics with wake inflow from the BEM solver with free wake analysis, and (*iii*) unsteady aerodynamic loads given directly from the 3D BEM potential formulation with a prescribed wake shape (see Equation (5)). In these analyses, the prescribed wake consists of the surface swept by the trailing edges of the blades during their motion. Note that, once the wake contribution in Equation (4) has been discretised using the approach described in Section 3.0, the wake effect is equivalent to that of a vortex-lattice with the presence of both trailed and shed vortices (see Ref. 11).

For advance ratio $\mu = 0{\cdot}15$, Figs 7-10 depict the comparisons between the results from the aerodynamic model using Drees wake inflow (baseline) and those from the models mentioned above. In Figs 7-9 the comparisons are presented in terms of lag, flap and torsion blade tip deformations, whereas Fig. 10 shows the comparison among the corresponding vibrating hub loads.

Blade tip displacements predicted by the two approaches using 2D quasi-steady aerodynamics with wake inflow from BEM solver are quite similar. They show a 1/rev oscillation of the flap deflection that is much larger than that given by the linear Drees wake inflow, although the mean value is similar. A slightly larger 1/rev oscillation is present also in the lag displacement, whereas the torsion deflection shows 3/rev oscillations that cannot be observed in the prediction from the linear inflow. Larger differences among the results from the three wake inflow models examined appear in the comparison concerning the 4/rev vibrating hub loads. Figure 10 shows that the vibrating hub loads predicted by the linear inflow are strongly underestimated with respect to those given by the computed wake inflows, and this is particularly evident for the out-of-plane loads. However, quite large differences appear also in the comparison between prescribed-wake and free-wake inflows. In general, loads predicted by the free-wake model are greater than those given by the prescribed one and, again, the out-of-plane loads are those showing the largest discrepancies. The differences in terms of vibrating hub loads between the results from the computed wake inflows seem to be not corresponding to the very similar tip displacement predictions in Figs 7 and 8. This is due to the fact that the 4/rev vibrating hub loads are given by combination of 3/rev, 4/rev and 5/rev load harmonics in the rotating frame, while the corresponding harmonics in the elastic displacements are difficult to observe, since these are dominated by the lower frequency motion. For the same reason the free-wake model yields greater vibrating hub loads than the prescribed-wake one: wake deformations affect higher harmonics of the aeroelastic solution and thus have a lower impact on the displacement prediction rather than on the calculation of the vibrating hub loads. These results confirm the well-known important role played by wake effects in the aeroelastic solution, and demonstrate that the need of a free-wake solver is particularly felt if the analysis is not limited to the determination of the blade elastic response, but is also delivered to the calculation of the vibrating hub loads.

The aeroelastic solution from the 3D BEM solver is depicted in Fig. 9. The flap and lag displacements are not much different from those given in Figs 7 and 8, although a bit smaller 1/rev flap and lag oscilla-

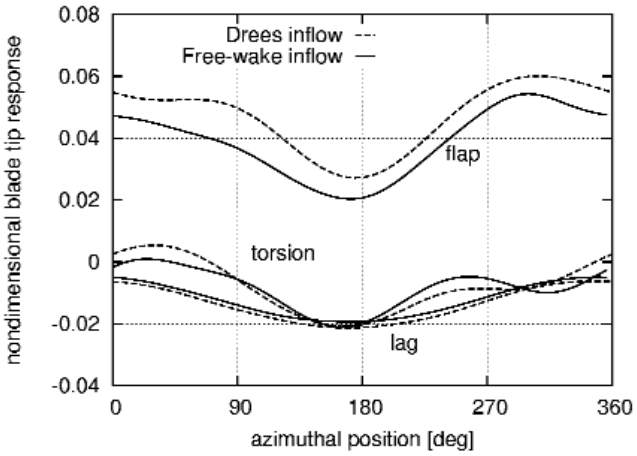


Figure 12. Blade deformation: linear inflow *vs* free-wake inflow ($\mu = 0{\cdot}30$).

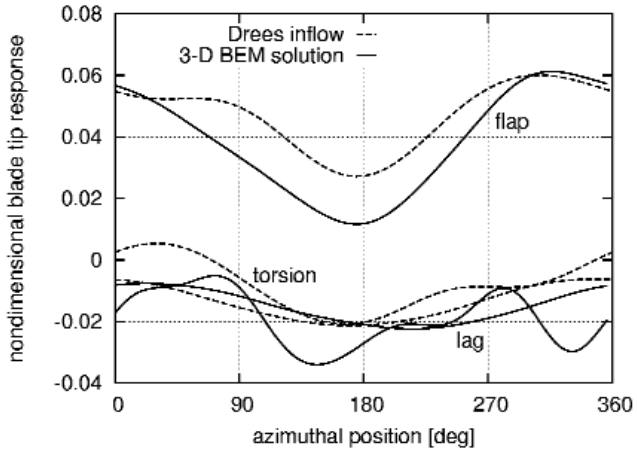


Figure 13. Blade deformation: linear inflow *vs* 3D BEM solution ($\mu = 0{\cdot}30$)

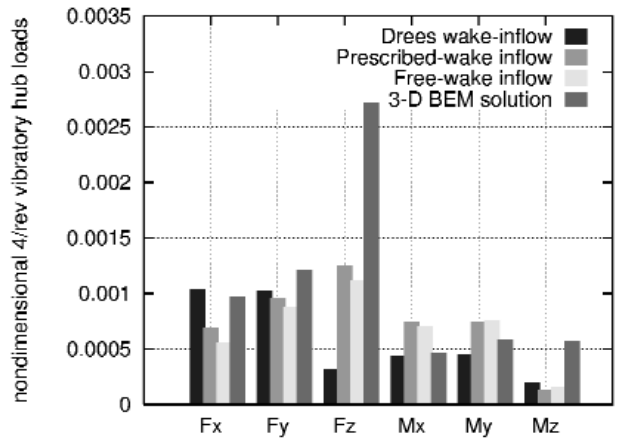


Figure 14. 4/rev hub loads ($\mu = 0{\cdot}30$).

https://doi.org/10.1017/S0001924000001664 Published online by Cambridge University Press

tions and a bit larger (negative) lag mean value are present. However, the most peculiar aspect of the 3D BEM solution is represented by the large oscillations of the torsion deflection that are dominated by the 3/rev harmonic. As a consequence, the corresponding in-plane vibrating hub loads depicted in Fig. 10 are significantly greater than those predicted by the aeroelastic model using the wake inflow from the same prescribed wake shape, whereas the out-of-plane loads are smaller (in particular, the force in the direction of the axis of rotation). The in-plane vibrating hub loads predicted by the free-wake inflow are comparable with those given by the 3D BEM solution, while the out-of-plane loads are much higher. The differences between the aeroelastic solution from the 3D BEM solver and the solution using the wake inflow from prescribed wake, arise from the fact that in the latter case the flow 3D and unsteadiness effects are taken into account only through the wake inflow contribution, whereas the relation between body velocity and airloads is that predicted by the 2D quasi-steady solution. The identification of the influence of the effects that are missing in this type of solver is not an easy task, and depends on the specific configuration examined. The results shown here demonstrate that in the problem analyzed they have an important role in the torsion prediction. It is worth noting that when numerical predictions from aeroelastic models using 2D quasi-steady aerodynamics coupled with free-wake inflow are compared with experimental measurements a significant underestimation of the oscillations of the torsion deflection is revealed (see, for instance, Refs 23 and 24).

Finally, the helicopter rotor flying at advance ratio $\mu = 0{\cdot}30$ is examined. In this case, the rotor quickly moves far away from its wake and thus, with respect to the case at $\mu = 0{\cdot}15$, the wake shape plays a minor role in aeroelastic predictions. This fact is demonstrated by Figs 11, 12 and 14 that show that not only blade tip displacements are almost identically predicted by the aeroelastic solvers based on the prescribed-wake and the free-wake inflows (akin to what observed for the case at $\mu = 0{\cdot}15$), but in this case also the vibrating hub loads predicted using the two wake inflow models are very similar (the differences with respect to the linear inflow solution are also smaller). Figure 13 depicts the 3D BEM solution. At this advance ratio it predicts flap and lag displacements that are quite close to those given by the solutions from the computed wake inflows (with the lag showing a small phase shift). The torsion deflections from the 3D BEM solver are still more oscillating than those from prescribed-wake and free-wake inflows, but in this case the difference is alleviated. It has a significant 4/rev harmonic content and this produces the high values of the out-of-plane vibrating hub loads shown in Fig. 14, while the in-plane loads are closer to those given by the other solvers examined. In the overall, at $\mu = 0{\cdot}30$ the differences among predictions from the 3D BEM solver and predictions from prescribed-wake and the free-wake inflows appear to be reduced with respect to what observed at the smaller advance ratio.

6.0 CONCLUDING REMARKS

For helicopter rotors in forward flight, a nonlinear structural model has been coupled with a three-dimensional, unsteady, aerodynamic solver based on a BEM potential-flow formulation. The aeroelastic equations have been integrated by applying the Galerkin method, followed by a harmonic balance approach. The BEM solver has been applied both for the direct evaluation of unsteady blade loads and for the evaluation of the wake inflow to be combined with a quasi-steady section aerodynamics model. It yields a unified approach for aeroelastic response and blade pressure prediction that is of interest for aeroacoustic purposes. The numerical investigation on a four-bladed helicopter rotor in forward flight has started with the validation of the solution procedure, and then has analyzed the influence of aerodynamic modeling on aeroelastic predictions at two advance ratios.

At low advance ratio, the aeroelastic solution shows a significant dependence on the aerodynamic modeling. In particular, for the aeroelastic solvers using wake inflows, the prediction of the vibrating hub loads is significantly influenced by the wake model used in the computation of the inflow. Predictions from the 3D BEM solver differ from those given by models based on 2D quasi-steady aerodynamics. The difference is particularly evident in terms of torsion deflection oscillations. However, also the vibrating hub loads predicted show significant discrepancies. It is worth noting that the literature yields examples of comparisons between numerical predictions from aeroelastic models using 2D quasi-steady aerodynamics coupled with free-wake inflow and experimental measurements that show a significant underestimation of the oscillations of the torsion deflection.

At high advance ratio the aeroelastic response is less influenced by the wake and the predictions from the different models show a better agreement. In this case, also the 3D BEM solution is closer to the other solutions examined, although a more oscillating behavior of the torsion deflection is still present, and consequently higher values of the vibrating hub loads (the in-plane ones, in particular) are predicted.

In general, the numerical analysis has demonstrated that the aerodynamic modeling has a significant impact both on blade response and hub load predictions. Different results are obtained by the application of quasi-steady airloads coupled with different wake inflows, and larger discrepancies are observed in the comparison with the 3D BEM solutions. Particular attention should be paid on the remarkable differences arising between the results from the 2D section airload model with prescribed-wake inflow and the 3D BEM solutions that are derived from the same wake shape. Indeed, the BEM solutions capture three-dimensional, unsteadiness and blade shape effects more accurately than the 2D section airload model enhanced with inclusion of wake inflow. However, the question on the differences observed is still open and needs additional research activity. For instance a comparative study with experimental data would be useful, but it is beyond the aim of the present work.

REFERENCES

1. LIM, J.W., YU, Y.H. and JOHNSON, W. Calculation of rotor blade-vortex interaction airloads using a multiple-trailer free-wake model, *J Aircr* 2003, **40**, (6), pp 1123-1130.
2. MUNSKY, B., GANDHI, F. and TAUSZIG, L. An analysis of helicopter blade-vortex interaction noise with flight path or attitude modification, 58th Annual Forum of the American Helicopter Society, 2002, Montreal, Canada.
3. LIU, L., PATT, D. and FRIEDMANN, P.P. Simultaneous vibration and noise reduction in rotorcraft using aeroelastic simulation, 60th Annual Forum of the American Helicopter Society, 2004, Baltimore, MD, USA.
4. PATT, D., LIU, L. and FRIEDMANN, P.P. Rotorcraft vibration reduction and noise predictions using a unified aeroelastic response simulation, *J American Helicopter Society*, 2005, **50**, (1), pp 95-106.
5. BEAUMIER, P. and DELRIEUX, Y. Description and validation of the ONERA computational methods for the prediction of blade-vortex interaction noise, *Aerospace Science and Technology*, 2005, **9**, pp 31-43.
6. DATTA, A. and CHOPRA, I. Validation and understanding of UH-60A vibratory loads in steady level flight, *J American Helicopter Society*, 2004, **49**, (3), pp 271-287.
7. HANSFORD, R.E. and VORWALD, J. Dynamics workshop on rotor vibratory loads prediction, *J American Helicopter Society*, 1998, **31**, (1), pp 76-87.
8. HODGES, D.H. and DOWELL, E.H. Nonlinear equation for the elastic bending and torsion of twisted nonuniform rotor blades, NASA TN D-7818, 1974.
9. MORINO, L. A general theory of unsteady compressible potential aerodynamics, NASA CR-2464, 1974.
10. GENNARETTI, M., CORSETTI, E. and MORINO, L. Coupled free-wake-aerodynamics/blade-dynamics analyses of rotors in forward flight, AIAA Paper 98-2241, 4th AIAA/CEAS Aeroacoustic Conference, May 1998, Toulouse, France.
11. GENNARETTI, M. and BERNARDINI, G. A novel potential-flow boundary integral formulation for helicopter rotors in BVI conditions, AIAA Paper 2005-2924, 11th AIAA/CEAS Aeroacoustic Conference, May 2005, Monterey, California, USA.

https://doi.org/10.1017/S0001924000001664 Published online by Cambridge University Press

12. MORINO, L., GENNARETTI, M. and PETROCCHI, P. A general theory of potential aerodynamics with applications to helicopter rotor-fuselage interaction, Symposium of the International Association for Boundary Element Methods, 1991, Kyoto, Japan.
13. HODGES, D.H. and ORMISTON R.A. Stability of elastic bending and torsion of uniform cantilever rotor blades in hover with variable structural coupling, NASA TN D-8192, 1976.
14. MORINO, L., KAPRIELIAN, Z., JR. and SIPCIC, S.R. Free wake analysis of helicopter rotors, *Vertica*, 1985, **9**, (2), pp 127-140.
15. GREENBERG, J.M. Airfoil in sinusoidal motion in a pulsating stream, NACA TN-1326, 1947.
16. THEODORSEN, T. General theory of aerodynamic instability and the mechanism of flutter, NACA Report 496, 1935.
17. DREES, J.M. A theory of airflow through rotors and its application to some helicopter problems, *J Helicopter Association of Great Britain*, 1949, **3**, (2), pp 79-104.
18. ZHANG, J. Active-Passive Hybrid Optimization of Rotor Blades with Trailing Edge Flaps, PhD Thesis, Department of Aerospace Engineering, The Pennsylvania State University, 2001.
19. BIR, G. and CHOPRA, I., *et al*. University of Maryland advanced rotor code (UMARC) Theory Manual, Technical Report UM-AERO 94-18, Center for Rotorcraft Education and Research, University of Maryland, College Park, 1994, Maryland, USA.
20. MORINO, L. and GENNARETTI, M. Boundary integral equation methods for aerodynamics, computational nonlinear mechanics in aerospace engineering, edited by ATLURI, S.N. *Progress in Aeronautics & Astronautics*, 1992, **146**, AIAA, Washington, DC, USA, pp 279-320.
21. GENNARETTI, M., LUCERI, L., and MORINO, L. A unified boundary integral methodology for aerodynamics and aeroacoustics of rotors, *J Sound and Vibrations*, 1997, **200**, (4), pp 467-489.
22. SCHULTZ, K.J., SPLETTSTOESSER, W., JUNKER, B., WAGNER, W., SCHOELL, E., ARNAUD, G., MERCKER, E., PENGEL, K. and FERTIS, D. A parametric wind tunnel test on rotorcraft aerodynamics and aeroacoustics (HELISHAPE) – Test Documentation and Representative Results, Proceedings of the 22nd European Rotorcraft Forum, September 1996, Brighton, UK.
23. BERNARDINI, G., SERAFINI, J., GENNARETTI, M. and IANNIELLO, S. Aeroelastic modeling effect in rotor BVI noise prediction, AIAA Paper 2006-2606, 12th AIAA/CEAS Aeroacoustics Conference, May 2006, Cambridge, MA, USA.
24. LIM, J.W., TUNG, C., YU, Y.H., BURLEY, C.L., BROOKS, T., BOYD, D., VAN DER WALL, B., SCHNEIDER, O., RICHARD, H., RAFFEL, M., BEAUMIER, P., BAILLY, J., DELRIEUX, Y., PENGEL, K. and MERCKER, E. HART II: Prediction of blade-vortex interaction loading, 29th European Rotorcraft Forum, September 2003, Friedrichshafen, Germany.

APPENDIX

This Appendix yields the stiffness matrix appearing in the Fourier-transformed aeroelastic equations, namely Equations (14) and (15). It is obtained by expressing the stiffness matrix in terms of the following Fourier series

$$\mathbf{K}(t) = \mathbf{K}_0 + \sum_{n=1}^{N} \left[\mathbf{K}_n^c \mathrm{Cos}(\Omega_n t) + \mathbf{K}_n^s \mathrm{Sin}(\Omega_n t) \right] \qquad \ldots (16)$$

and combining it with the harmonics of $\mathbf{q}$. The result is that the harmonics of the term $\mathbf{K}(t)\mathbf{q}$ in Equation (10) are given by $\hat{\mathbf{K}}\hat{\mathbf{q}}$ with

$$\begin{bmatrix}
\mathbf{K}_0 & \frac{1}{2}\mathbf{K}_1^c & \frac{1}{2}\mathbf{K}_1^s & \frac{1}{2}\mathbf{K}_2^c & \frac{1}{2}\mathbf{K}_2^s & \cdots \\
\mathbf{K}_1^c & \mathbf{K}_0 + \frac{1}{2}\mathbf{K}_2^c & \frac{1}{2}\mathbf{K}_2^s & \frac{1}{2}\left(\mathbf{K}_1^c + \mathbf{K}_3^c\right) & \frac{1}{2}\left(\mathbf{K}_1^s + \mathbf{K}_3^s\right) & \cdots \\
\mathbf{K}_1^s & \frac{1}{2}\mathbf{K}_2^s & \mathbf{K}_0 - \frac{1}{2}\mathbf{K}_2^c & -\frac{1}{2}\left(\mathbf{K}_1^s - \mathbf{K}_3^s\right) & \frac{1}{2}\left(\mathbf{K}_1^c - \mathbf{K}_3^c\right) & \cdots \\
\mathbf{K}_2^c & \frac{1}{2}\left(\mathbf{K}_1^c + \mathbf{K}_3^c\right) & -\frac{1}{2}\left(\mathbf{K}_1^s - \mathbf{K}_3^s\right) & \mathbf{K}_0 + \frac{1}{2}\mathbf{K}_4^c & \frac{1}{2}\mathbf{K}_4^s & \cdots \\
\mathbf{K}_2^s & \frac{1}{2}\left(\mathbf{K}_1^s + \mathbf{K}_3^s\right) & \frac{1}{2}\left(\mathbf{K}_1^c - \mathbf{K}_3^c\right) & \frac{1}{2}\mathbf{K}_4^s & \mathbf{K}_0 - \frac{1}{2}\mathbf{K}_4^c & \cdots \\
\vdots & \vdots & \vdots & \vdots & \vdots & \ddots
\end{bmatrix} \qquad \ldots (17)$$

where only the contribution of the lowest two harmonics is explicitly expressed. Similar expressions are derivable for $\hat{\mathbf{M}}$ and $\hat{\mathbf{C}}$.

https://doi.org/10.1017/S0001924000001664 Published online by Cambridge University Press